Specialized Conductor Models for Finite Element Eddy Current Simulation

Herbert De Gersem[1], Kay Hameyer[2], Thomas Weiland[1]
[1]Technische Universität Darmstadt, Computational Electromagnetics Laboratory (TEMF),
Schloßgartenstraße 8, D-64289 Darmstadt, Germany
phone: +49 6151 162361 / fax: +49 6151 164611
degersem/weiland@temf.tu-darmstadt.de; www.temf.de
[2]Katholieke Universiteit Leuven, Dep. ESAT, Div. ELECTA,
Kasteelpark Arenberg 10, B-3001 Leuven-Heverlee, Belgium
phone: +32 16 321020 / fax: +32 16 321985
kay.hameyer@esat.kuleuven.ac.be; www.esat.kuleuven.ac.be/elen/elen.html

Keywords

Modelling, simulation

Abstract

Transformer and machine windings with complicated shapes and winding schemes can not be considered in full detail within an overall machine model. In this paper, besides the standard solid and stranded conductor models, specialized conductor models are developed for foil and machine windings which may exhibit particular skin and proximity effects. The conductor models globally behave as the true windings without requiring a full geometrical discretization or detailed winding scheme. They refine adaptively according to local error estimates in the global model, offer smaller computational times and are more reliable than if solid and stranded conductor models would be applied. The conductor models appear as magnetically coupled elements in an external circuit model. The field-circuit coupled model is conveniently represented by a coupled system of equations.

Introduction

Windings applied in transformers and rotating machine can have very complicated geometries and sophisticated winding schemes. Not only intentional eddy current effects aiming at forces or heat generation but also unintentional eddy current effects giving rise to local stress accumulation and hot spots inside the windings have to be simulated accurately.

Two model scales are distinguished: the *macro scale*, i.e. at the global model and considering the fundamental machine behaviour, and the *micro scale*, i.e. inside the winding and dealing with skin and proximity effects with smaller wave lengths. The magnitude of induced phenomena does not only depend on the properties of the winding itself but also on the vicinity of highly permeable materials or moving parts and the spectrum of the applied excitation. Therefore, in general, phenomena at macro-scale can not be decoupled from phenomena at micro-scale. The straightforward approach accounting for micro-scale effects requires a discretization of the entire machine up to micro-scale dimensions. This, however, yields huge models and unacceptable simulation times.

Several model reduction techniques are developed in order to introduce micro-scale effects in global models: e.g. analytical macro-elements [7] and inner node elimination techniques [11]. They constitute a-priori model reductions, which are troublesome in case of non-linear materials and may hinder adaptive error control during finite element (FE) simulation. In this paper, we propose to approximate the detailed geometries and winding schemes by additional discretizations for the voltage and to insert these into the magnetic FE model. An error estimator automatically updates the multi-conductor model during the simulation.

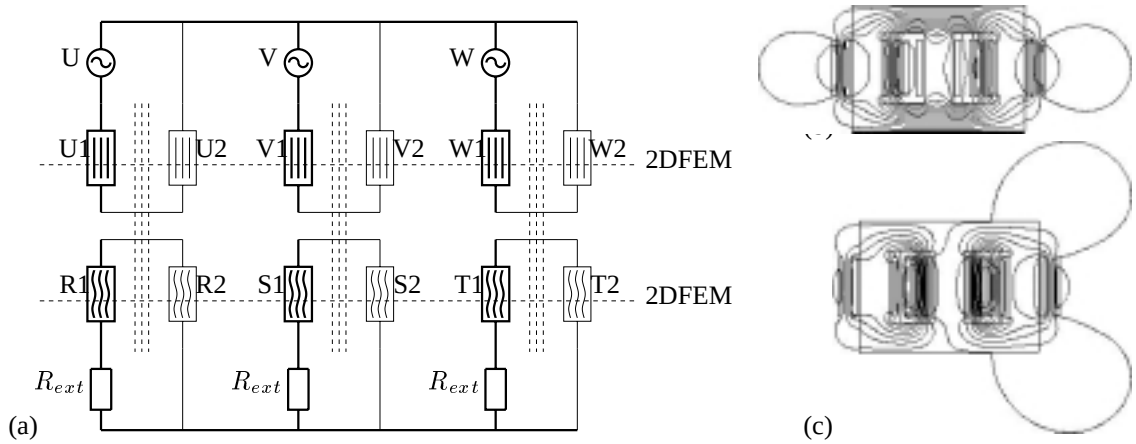

Fig. 1. Three-phase foil-winding transformer: (a) external circuit model part and FE model part with magnetic flux lines (b) t_0 and (c) $t_0 + T/4$ (U1-W2 are stranded conductors whereas R1-T2 are foil conductors).

Magnetodynamic finite element model

Eddy current phenomena are described by the partial differential equation (PDE)

$$\nabla \times (\nu \nabla \times \mathbf{A}) + \sigma \frac{\partial \mathbf{A}}{\partial t} = -\sigma \nabla V \tag{1}$$

in terms of the magnetic vector potential $\mathbf{A}$, the voltage V, the reluctivity ν and the conductivity σ. Here, as an example, a 2D time-harmonic formulation is used:

$$-\frac{\partial}{\partial x}\left(\nu \frac{\partial \underline{A}_z}{\partial x}\right) - \frac{\partial}{\partial y}\left(\nu \frac{\partial \underline{A}_z}{\partial y}\right) + \jmath\omega\sigma \underline{A}_z = -\sigma \frac{\partial \underline{V}}{\partial z} \tag{2}$$

with $\underline{A}_z$ the phasor of the z-component of $\mathbf{A}$, ω the pulsation and $\underline{V}$ the phasor of the voltage. This formulation is commonly applied for devices with a translatory symmetry in the z-direction. The voltage drops and the currents are assumed to be perpendicular to the cross-section of the coils with the FE model. The dependence of the voltage $\underline{V}(x, y)$ and the current density $\underline{J}_z(x, y)$ on the spatial coordinates x and y of the considered cross-sections depends on the applied conductor model as will become clear in the next section. The 2D FE model of the cross-section Ω_{fe} of the device is extended with an equivalent circuit modelling the electric connections at the front and rear machine ends and the external sources and loads [12] (Fig. 1). The restriction to 2D time-harmonic models substantially facilitates the expressions describing the conductor models considered in this paper. However, only small modifications are required in order to apply the specialized conductor models to 3D and transient formulations as well.

The discretization of (2) by n_{fe} linear triangular FE shape functions $N_i(x, y)$ yields the system of equations

$$(K_{\mathrm{fe}} + \jmath\omega L_{\mathrm{fe}})\, \underline{u} + \underline{f} = 0 \tag{3}$$

with $\underline{u}$ containing the degrees of freedom for $\underline{A}_z$,

$$K_{\mathrm{fe},ij} = \int_\Omega \left(\nu \frac{\partial N_i}{\partial x}\frac{\partial N_j}{\partial x} + \nu \frac{\partial N_i}{\partial y}\frac{\partial N_j}{\partial y}\right) \mathrm{d}\Omega \; ; \tag{4}$$

$$L_{\mathrm{fe},ij} = \int_\Omega \sigma N_i N_j \, \mathrm{d}\Omega \; . \tag{5}$$

The load term $\underline{f}$ will be further specified in the next section.

Conductor models

The current distribution in a conductor submitted to a time-varying magnetic field is characterized by the *skin depth*

$$\delta = \sqrt{\frac{1}{\pi f \mu \sigma}} \,. \tag{6}$$

The skin depth depends on the conductivity σ and the permeability μ of the conductor material and the frequency f of the time-varying magnetic field. The skin depth is the thickness of the layer of a conductive plane in which the majority of the current is concentrated. The skin depth gives an indication of the importance of eddy current effects, even for conductors with arbitrary geometries. The dimensions of the cross-sections of the coils, wires and bars present in the FE model are characterized by the lengths d_x and d_y with respect to the x- or y-direction respectively. d_x and d_y are compared to the skin depth (Fig. 2A). If one of both is considerably smaller than δ, the technical conductor model may neglect the current redistributed with respect to the corresponding direction. Several conductor models are distinguished (Fig. 3). The solid and stranded conductor models are commonly applied in FE models and form the limit cases for very large and very small ratio's d_x/δ and d_y/δ. Conductors that do not carry current and expel all almost all incident flux can be modelled by impedance boundary conditions applied at their boundaries [13]. In this paper, two novel conductor models, the *foil conductor* and *multi-conductor* model, are added to the possible models for magnetically coupled conductors. The foil and multi-conductor models enable the application of relatively small models for windings with confined skin effect for which otherwise a large interconnected set of solid conductor models would be required. The foil conductor model is a special case of a multi-conductor model but is treated separately because of its direct relation to foil windings. In this section the different conductor models are described. They are inserted into an external electrical circuit as shown in the next section.

Solid conductor model

The voltage drop applied to a massive conductor with the cross-section $\Omega_{\rm sol}$ with the FE model is constant over $\Omega_{\rm sol}$: $\Delta\underline{V}(x,y) = \Delta\underline{V}_{\rm sol}$. For the 2D models considered here, this follows directly from the assumptions that:

- the model length is significantly larger than the characteristic length corresponding to the magnetic behaviour within the 2D cross-section of the model;
- the differences in conductivity between conductors and non-conductors are substantial;
- the voltages are constant at the front and rear cross-sections of the conductors.

The load term of (2) due to the excited solid conductor is related to the voltage drop $\Delta\underline{V}_{\rm sol}$ by $\underline{f}_i = Q_{i,\rm sol}\Delta\underline{V}_{\rm sol}$ with

$$Q_{iq} = -\int_{\Omega_{\rm sol}} \frac{\sigma}{\ell_z} N_i \mathrm{d}\Omega \tag{7}$$

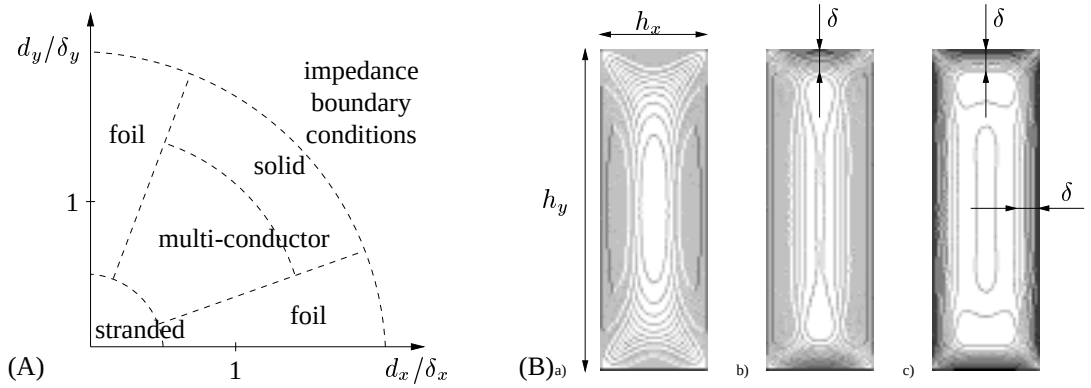

Fig. 2. (A) Application area of the several conductor models and (B) magnetic flux lines in a (a) stranded, (b) foil and (c) solid conductor.

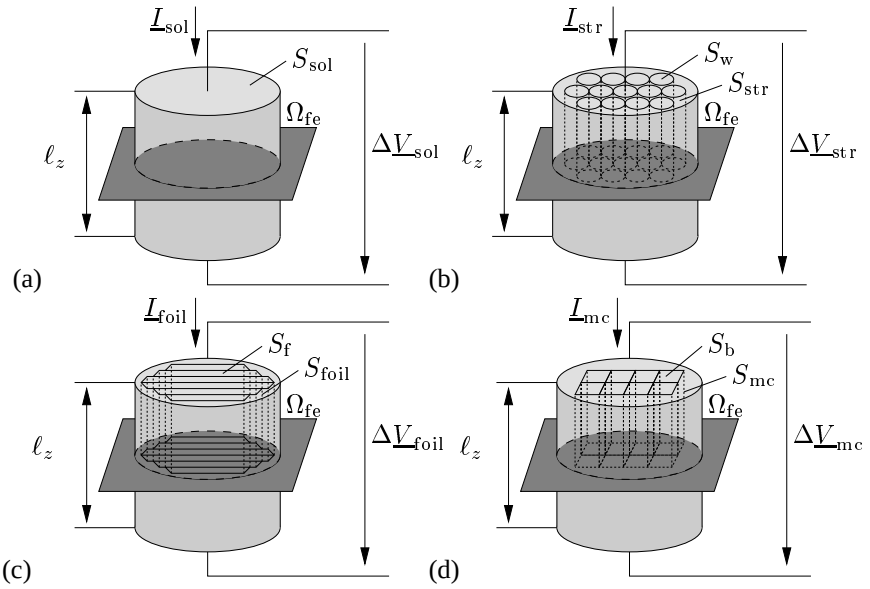

Fig. 3. (a) Solid conductor, (b) stranded conductor, (c) foil conductor and (d) multi-conductor models.

and ℓ_z the length of the model in the z-direction. Submitted to a time-varying magnetic field represented by the z-component of the magnetic vector potential, the solid conductor experiences a current density

$$\underline{J}_z(x,y) = \frac{\sigma}{\ell_z}\Delta\underline{V}_{\rm sol} - \jmath\omega\sigma\underline{A}_z(x,y)\ . \tag{8}$$

The total current through the conductor is related to the applied voltage drop and the magnetic field by

$$\underline{I}_{\rm sol} = G_{\rm sol}\Delta\underline{V}_{\rm sol} + \jmath\omega\ell_z\sum_{j=1}^{n_{\rm fe}} Q_{j,{\rm sol}}\underline{u}_j\ ; \quad G_{\rm sol} = \int_{\Omega_{\rm sol}}\frac{\sigma}{\ell_z}{\rm d}\Omega \tag{9}$$

with $G_{\rm sol}$ the DC admittance of the solid conductor and $Q_{j,{\rm sol}}$ defined by (7). The FE model of a single solid conductor excited by a current source with current $\underline{I}_{\rm src}$ reads

$$\begin{bmatrix} K+\jmath\omega L & Q \\ Q^T & \chi G_{\rm sol}\end{bmatrix}\begin{bmatrix}\underline{u}\\ \Delta\underline{V}_{\rm sol}\end{bmatrix} = \begin{bmatrix}0\\ \chi\underline{I}_{\rm src}\end{bmatrix} \tag{10}$$

with $\chi = 1/\jmath\omega\ell_z$ a factor applied in order to symmetrize the block system of equations.

Stranded conductor model

In many devices, windings with a considerable number of wires, connected in series or parallel, are used. The diameters of the wires are smaller than the skin depth according to the applied frequencies and materials. However, the extent of the cross-section of the entire winding may exceed δ. The treatment of each separate wire as a solid conductor would require the geometrical details of all wires to be resolved in the mesh. Moreover, one unknown $\Delta\underline{V}_{\rm sol}$ and one integral relation of the form (9) per wire would have to be added to the coupled system of equations. This substantially increases the size of the system to be solved and therefore reduces the efficiency of the simulation. Instead, a modelling assumption is introduced. As δ exceeds the dimension of each of the wires, the current density may be assumed to be constant within the cross-section of each wire and, because the wires are connected in series, within the cross-section of the entire winding. The cross-section $\Omega_{\rm str}$ of the stranded conductor with the FE model includes all wires, insulation materials and cooling ducts. Two cross-sections of the same coil and the FE plane but with opposite orientation, have to be treated as separate stranded conductors and appropriately coupled through an external electric circuit as described in the next section. Eddy current phenomena inside the winding are neglected by omitting the $\jmath\omega I_{{\rm fe},ij}$ coefficients in (3) for all FE nodes i and j contained in $\Omega_{\rm str}$. The current density $\underline{J}_{\rm str}$ is related to the current $\underline{I}_{\rm str}$ supplying the stranded conductor by the expression

$$\underline{J}_{\rm str} = \frac{N_{\rm str}}{S_{\rm str}}\underline{I}_{\rm str} \tag{11}$$

with $N_{\rm str}$ the number of turns and $S_{\rm str}$ the surface of $\Omega_{\rm str}$. The load term $\underline{f}$ due to the excited stranded conductor is given by $\underline{f}_i = P_{i,\rm str}\underline{I}_{\rm str}$ with

$$P_{i,\rm str} = -\int_{\Omega_{\rm str}} \frac{N_{\rm str}}{S_{\rm str}} N_i \mathrm{d}\Omega \ . \tag{12}$$

The voltage drop over the entire stranded conductor is the sum of the voltage drops over each of the wires. In the continuous model, developed here, this summation is replaced by an integral over $\Omega_{\rm str}$ averaging the voltage drop over the cross-section of the stranded conductor:

$$\Delta\underline{V}_{\rm str} = \frac{1}{S_{\rm str}} \int_{\Omega_{\rm str}} \ell_z \left(\frac{\underline{J}_z(x,y)}{f_{\rm str}\sigma} + \jmath\omega\underline{A}_z(x,y) \right) \mathrm{d}\Omega \ ; \quad f_{\rm str} = \frac{N_{\rm str}S_{\rm w}}{S_{\rm str}} \tag{13}$$

with $f_{\rm str}$ the fill factor accounting for the necessary correction of the overall conductivity due to the presence of insulation and gaps. $S_{\rm w}$ is the surface of the cross-section of a single wire. The total voltage drop along the winding is

$$\Delta\underline{V}_{\rm str} = R_{\rm str}\underline{I}_{\rm str} - \jmath\omega\ell_z \sum_{j=1}^{n_{\rm fe}} P_{j,\rm str}\underline{u}_j \ ; \quad R_{\rm str} = \int_{\Omega_{\rm str}} \frac{N_{\rm str}\ell_z}{\sigma S_{\rm w}} \tag{14}$$

with $R_{\rm str}$ the DC resistance of the stranded conductor and $P_{j,\rm str}$ defined by (12). This approach yields the *stranded* (or *filamentary*) *conductor model* for a winding. The model is a continuous idealization and behaves as if the discrete number of wires were replaced by an infinite set of infinitely thin solid conductors. This is the modelling assumption introduced by the stranded conductor paradigm. A single stranded conductor excited by a voltage source with voltage $\underline{V}_{\rm src}$ is modelled by the block system of equations

$$\begin{bmatrix} K & P \\ P^T & -\chi R_{\rm str} \end{bmatrix} \begin{bmatrix} \underline{u} \\ \underline{I}_{\rm str} \end{bmatrix} = \begin{bmatrix} 0 \\ -\chi\Delta\underline{V}_{\rm src} \end{bmatrix} \tag{15}$$

where in this case the relation (14) has to be multiplied by $-\chi$ in order to obtain symmetry.

A stranded conductor model with cross-section $\Omega_{\rm str}$ only models one of both winding parts of the coil crossing the FE model. As a consequence, the voltage drop $\Delta\underline{V}_{\rm str}$ expressed by (14) only represents one part of the voltage drop over the entire coil. The external electric circuit model described in the next section will connect two stranded conductor models in series representing a single coil. The voltage drop along both stranded conductors is in general different due to different magnetic vector potentials at both coil cross-sections. The induced voltage drops represented by $\jmath\omega\underline{A}_z$ in (14), however, have no physical meaning unless they are added in which case they reflect the voltage drop induced by the time-varying magnetic field enclosed by the coil.

Foil Conductor Model

Foil windings are applied in transformers and heating devices. A foil winding consists of a conductive foil wound around a core (Fig. 4b). An alternating current applied to the foil conductor is redistributed towards the tips of the conductor but not in the perpendicular direction (Fig. 4c). The insulation enables a change of the voltage drop only in the perpendicular direction (Fig. 4d). In contrast to massive bars and common wire windings, foil windings experience a skin effect only in the longitudinal direction with respect to the foils (Fig. 2B).

Both the solid and stranded conductor model are not suited for simulating foil windings. In theory, the simulation of a foil winding requires to treat the foil winding by a series connection of a large number of solid conductor models. Since the cross-section of each foil is a small and long rectangle, the FE discretization requires a too fine or very specialized mesh. Although the voltages along neighbouring foils are very close, the field-circuit coupled model incorporates one unknown voltage per foil. The large number of degrees of freedom, both in the FE model and in the external circuit, results in an inefficient simulation.

Consider a winding of $N_{\rm foil}$ foils, wound around a vertical core and connected in series. The cross-section of the foil winding with the FE plane has an extent $\Delta y = y_2 - y_1$ in the y-direction and an

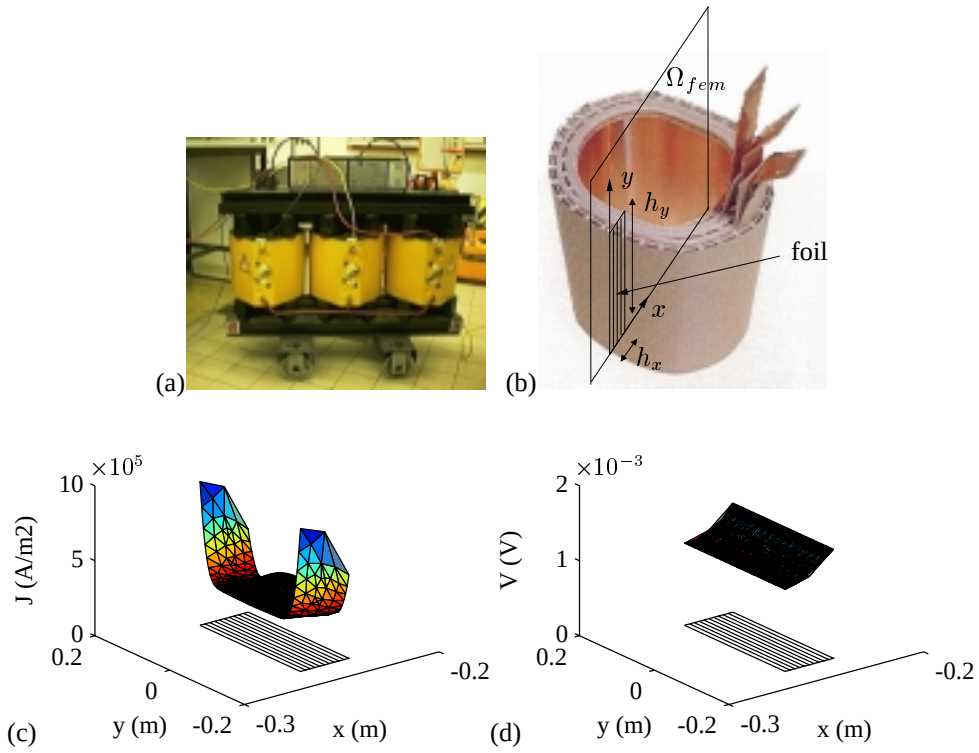

Fig. 4. (a) Foil-winding distribution transformer (rated power 30 kVA; rated voltages 400/3000 V; rated currents 43.5/5.8 A; rated frequency 50 Hz; connection Yy) (Pauwels Trafo Belgium N.V.); (b) foil winding; (c) current density in and (d) voltage across the foils of one of the foil windings of the transformer (the foil mesh is plotted in the xy-base plane).

extent $\Delta x = x_2 - x_1$ in the x-direction. Δy exceeds the skin depth considerably whereas $\Delta x / N_{\text{foil}}$ is smaller than δ. The specialized foil conductor model presented in this paper relies upon an additional 1D discretization for the voltage drop applied in the direction of the change in voltage drop [2]. The voltage drop is discretized by

$$\Delta \underline{V}(x,y) = \sum_{q=1}^{n_{\text{foil}}} M_q(x) \underline{v}_q \tag{16}$$

with $M_q(x)$ a *foil shape function* (FSF), n_{foil} is the number of FSFs and $\underline{v}_q$ a degree of freedom. A FSF has a constant value in the y-direction and local support in the x-direction (Fig. 5a). The support of a FSF is a long rectangle and thus has a similar shape as a single foil itself. A FSF, however, may overlap several foils. The supports of the FSFs do not necessarily match the true foil geometry. The voltages along N_{foil} foils are represented by n_{foil} unknowns $\Delta \underline{V}_g$. If N_{foil} is large and the voltages do not vary too rapidly along the x-cross-section of the foil winding, choosing $n_{\text{foil}} << N_{\text{foil}}$ offers a significant reduction of the number of unknowns in the model while retaining a sufficient accuracy. The *foil mesh*, i.e. the set of all FSFs, does also not coincide with the magnetic mesh. Adaptive mesh refinement can be applied independently. The FEs are refined based on the error estimation of the local magnetic field and the current density, yielding considerable refinement at the tips of the foils. The error estimator for the FSFs weighs the voltage variation between two successive foil elements and invokes refinement if that variation is too large.

The load term $\underline{f}$ is $\underline{f}_i = \sum_{q=1}^{n_{\text{foil}}} Z_{iq} \underline{v}_q$ with

$$Z_{iq} = \int_\Omega \frac{\sigma}{\ell_z} N_i M_q \mathrm{d}\Omega \ . \tag{17}$$

a hybrid mass matrix combining the triangular shape functions $N_i(x,y)$ and the foil shape functions $M_g(x)$. Since the foil are connected in series, the current in each foil is the same. Similarly as in the case of a stranded conductor, a continuous model is applied. The constant current condition per foil is replaced by a constant current condition along the x-direction. The surface current in the cross-section

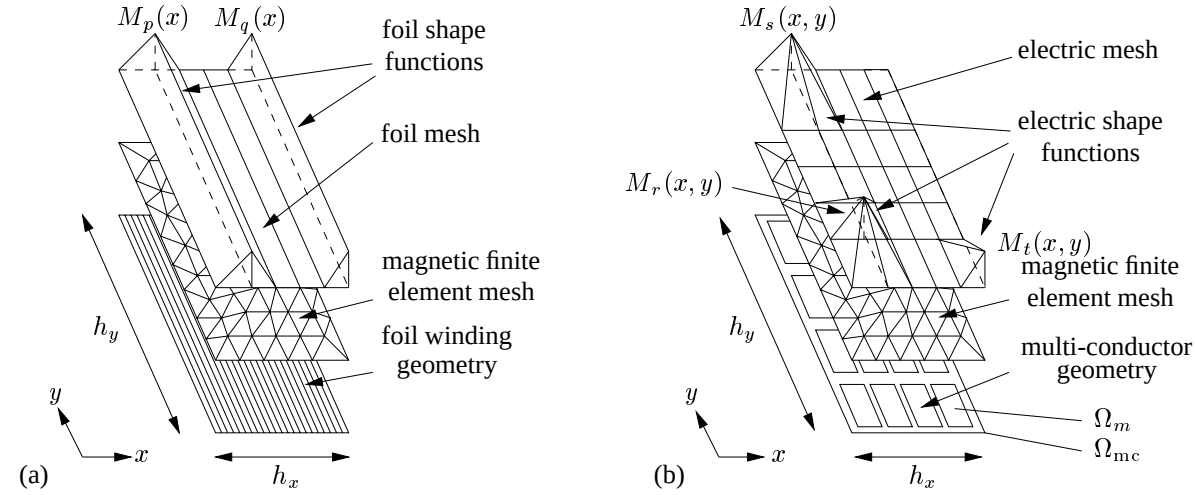

Fig. 5. Cross-section of the (a) foil winding and (b) multi-conductor, showing the magnetic mesh, the electric mesh and a few electric shape functions.

of the foil conductor with an yz-plane is

$$\underline{a}_{\mathrm{foil}}(x) = \int_{y_1}^{y_2} \underline{J}_z(x,y)\mathrm{d}y \tag{18}$$

The current density in the foil is

$$\underline{J}_z(x,y) = \frac{\sigma f_{\mathrm{foil}}}{\ell_z}\Delta\underline{V}(x) - \jmath\omega\sigma\underline{A}_z(x,y)\ ; \quad f_{\mathrm{foil}} = \frac{N_{\mathrm{foil}}S_{\mathrm{f}}}{S_{\mathrm{foil}}} \tag{19}$$

with f_{foil} the foil fill factor accounting for insulation and cooling ducts between the individual foils. The continuous constraint on the foil current relates the surface current for all possible yz-cross-sections of the foil winding to the foil current $\underline{I}_{\mathrm{foil}}$:

$$\underline{a}_{\mathrm{foil}}(x) = \frac{N_{\mathrm{foil}}}{\Delta x}\underline{I}_{\mathrm{foil}} \tag{20}$$

with Δx the thickness of the foil winding. The foil current constraint is discretized by the Galerkin weighted residual approach using the foil shape functions as weighting functions. The combination of (18), (19) and (20) weighted by the foil shape function $M_p(x)$ yields

$$\jmath\omega\ell_z\sum_{j=1}^{n_{\mathrm{fe}}} Z_{jp}\underline{u}_j + \sum_{q=1}^{n_{\mathrm{foil}}} G_{pq}\underline{v}_q + S_p\underline{I}_{\mathrm{foil}} = 0\ ; \tag{21}$$

$$G_{pq} = \int_\Omega \frac{\sigma f_{\mathrm{foil}}}{\ell_z} M_p M_q \mathrm{d}\Omega\ ; \quad S_p = -\frac{N_{\mathrm{foil}}}{S_{\mathrm{foil}}}\int_\Omega M_p\mathrm{d}\Omega\ . \tag{22}$$

The individual foils of the foil winding are connected in series. The voltage drop along the foil winding equals the voltage drop along a single foil averaged over the foil winding's cross-section and multiplied by the number of turns:

$$\Delta\underline{V}_{\mathrm{foil}} = \frac{N_{\mathrm{foil}}}{S_{\mathrm{foil}}}\int_\Omega \Delta\underline{V}(x)\mathrm{d}\Omega \tag{23}$$

which after insertion of voltage drop distribution in terms of the foil shape functions reads:

$$\Delta\underline{V}_{\mathrm{foil}} = -\sum_{q=1}^{n_{\mathrm{foil}}} S_q\underline{v}_q\ . \tag{24}$$

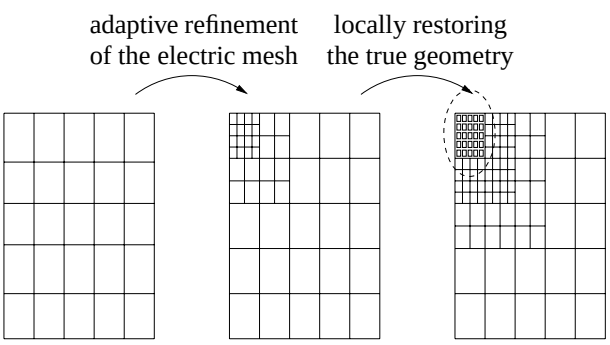

Fig. 6. Consistent adaptive refinement of the electric tensor grid when the error estimator indicates large variations of the voltage drop at the left upper corner of the multi-conductor cross-section (at a certain point, further refinement corresponds to restoring the original geometry).

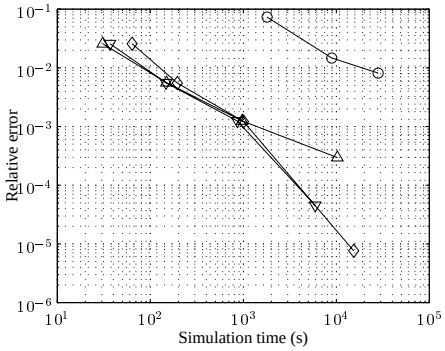

Fig. 7. Convergence of the global discretization error with respect to the the computation time: comparison between (o) the conventional series-connection of solid conductors and the foil winding models with (△) 6, (▽) 11 or (◊) 21 foil elements per foil winding.

The FE model including a single foil winding excited by a voltage source with voltage drop $\Delta\underline{V}_{\rm src}$ is represented by the block system of equations

$$\begin{bmatrix} K+\jmath\omega L & Z & 0 \\ Z^T & \chi G & \chi S \\ 0 & \chi S^T & 0 \end{bmatrix} \begin{bmatrix} \underline{u} \\ \underline{v} \\ \underline{I}_{\rm foil} \end{bmatrix} = \begin{bmatrix} 0 \\ 0 \\ -\chi\Delta\underline{V}_{\rm foil} \end{bmatrix} . \tag{25}$$

The factors χ and $-\chi$ are inserted to preserve the symmetry of the FE formulation.

General multi-conductor model

The multi-conductor model is a generalization of the foil conductor model for windings with dimensions in the wire's cross-section which are of the same order of magnitude as the skin depth (Fig. 2A). The voltage drop is discretized using more general voltage shape functions $M_f(x,y)$ (Fig. 5b) [3]. Similarly as for foil conductors, the condition of constant current per single wire is replaced by a continuous form. This condition is weighted by the voltage shape functions themselves. The formulation is completely equivalent to the formulation of the foil conductor model and is therefore not repeated here.

The electric mesh does not coincide with the magnetic mesh nor with the true multi-conductor geometry. The consistency of the discretization, however, requires the electric mesh to tend to the multi-conductor geometry if refinement is applied (Fig. 6). Also, the fill factor accounting for the fraction of insulation in the winding has to converge to 1. Hence, the gaps and the insulation regions disappear out of the support of the electric mesh causing the electric mesh to become disconnected.

Circuit Model

The FE conductor models described in the previous section are embedded in an external electric circuit together with voltage and current sources and passive circuit elements. The circuit may consist of several disconnected parts. A *loop* is a closed path through the circuit [1]. A *cut-set* is defined as a set of branches which upon removal would cause the number of disconnected circuit parts to increase by 1. A *tree* is a set of branches connecting all circuit nodes without forming loops. Tracing a tree through the circuit is done by selecting branches following a priority rule which will be defined below. The tree branches are called *twigs*, the remaining branches are called *links* and form the *co-tree*. A *fundamental cut-set* is formed by 1 twig and the unique set of links completing the cut-set. A *fundamental loop* consists of 1 link and the unique path through the tree closing the loop. The fundamental cut-sets and loops form maximal independent sets for the cut-sets and loops of the circuit respectively. The tree partitioning is algebraically represented by the *fundamental cut-set matrix* D and the *fundamental loop matrix* B containing the signed incidences of the circuit branches to the fundamental cut-sets and loops respectively. When the twigs are ordered first, the fundamental incidences matrices have the form

$$D = \left[\; I \quad D_{\rm tw,ln} \;\right] , \tag{26}$$

$$B = \left[\; B_{\rm ln,tw} \quad I \;\right] , \tag{27}$$

where the subscripts "tw" and "ln" indicate twigs and links or the associated fundamental cut-sets and loops respectively. A fundamental property of circuit theory is the relation $B_{\mathrm{ln,tw}} = -D^T_{\mathrm{tw,ln}}$ [1]. Applying the Kirchhoff current law (KCL) and the Kirchhoff voltage law (KVL) to the fundamental cut-sets and loops respectively results in the expressions

$$\begin{bmatrix} I & D_{\mathrm{tw,ln}} \end{bmatrix} \begin{bmatrix} \underline{I}_{\mathrm{tw}} \\ \underline{I}_{\mathrm{ln}} \end{bmatrix} = \begin{bmatrix} 0 \\ 0 \end{bmatrix}, \tag{28}$$

$$\begin{bmatrix} B_{\mathrm{ln,tw}} & I \end{bmatrix} \begin{bmatrix} \Delta\underline{V}_{\mathrm{tw}} \\ \Delta\underline{V}_{\mathrm{ln}} \end{bmatrix} = \begin{bmatrix} 0 \\ 0 \end{bmatrix}, \tag{29}$$

with $\underline{I}$ and $\Delta\underline{V}$ denoting currents and voltage drops. Because the fundamental cut-sets and fundamental loops form linear independent sets, the relations in (28) and (29) are not over-determined as would be the case if a Tableau analysis would be applied. The circuit theory recalled here, does not restrict to electrical circuits. It can also be applied to e.g. magnetic and thermal circuits.

Five categories of circuit branches are distinguished based on the form of the relation between the voltage drop and the current of the branch:

- For an *independent voltage source*, the voltage drop is known a priori.
- For a *voltage-driven branch*, it is possible to express the voltage-current relation by

$$\underline{I}_{\mathrm{br}} = G_{\mathrm{br}}\Delta\underline{V}_{\mathrm{br}} + \underline{q}_{\mathrm{br,coup}} \tag{30}$$

where G_{br} is the DC conductance of the branch and $\underline{q}_{\mathrm{br,coup}}$ is a coupling term.

- For a *voltage/current-driven branch*, both expressions (30) and (31) are applicable.
- For a *current-driven branch*, the voltage-current relation is of the form

$$\Delta\underline{V}_{\mathrm{br}} = R_{\mathrm{br}}\underline{I}_{\mathrm{br}} + \underline{p}_{\mathrm{br,coup}} \tag{31}$$

with R_{br} the DC resistance of the branch and $\underline{p}_{\mathrm{br,coup}}$ a coupling term.

- For an *independent current source*, the current is known a priori.

Branches are selected to participate to the tree in the order of priority indicated by the list above. To each circuit part, the following procedure is applied. The *set of connected nodes* collects all nodes that are already connected by the tree tracing procedure and initially consists of one arbitrarily chosen node. The *set of adjacent branches* contains all branches of which one vertex is connected. The tree is constructed by successively selecting the adjacent branch with the highest priority. The new twig is removed from the set of adjacent branches and its node that was not yet connected, is added to the set of connected nodes. Adjacent branches which are incident to this node, are removed from the set of adjacent branches whereas other branches incident to this node have to be removed. By construction, the priority of a twig is greater or equal to the priority of all links belonging to the associated fundamental cut-set. Similarly, the priority of a link is less or equal to the priorities of the twigs of the corresponding fundamental loop. This procedure favours voltage-driven branches and current-driven branches to be selected as twigs and links respectively. Voltage/current-driven branches take over the properties of voltage-driven branches or current-driven branches depending whether they are selected for the tree or the co-tree respectively. The exceptional cases when independent voltage and current sources show up in the co-tree and the tree respectively, deserve a special treatment. If an independent voltage source appears in the co-tree, the corresponding fundamental loop only contains independent voltage sources. If the KVL is satisfied for this loop, the independent-voltage-source link can be omitted. Otherwise, the circuit problem has no solution. An analogous reasoning applies to the cut-set associated with an independent-current-source twig.

The circuit branches are indexed and sorted in the following order: independent-voltage-source twigs (subscript "twv"), voltage-driven twigs (subscript "two"), current-driven twigs (subscript "twu"), voltage-driven links (subscript "lnu"), current-driven links (subscript "lno") and independent-current-source links (subscript "lni"). The fundamental cut-set and loop matrices are partitioned accordingly:

$$D = \begin{bmatrix} I & 0 & 0 & D_{\mathrm{twv,lnu}} & D_{\mathrm{twv,lno}} & D_{\mathrm{twv,lni}} \\ 0 & I & 0 & D_{\mathrm{two,lnu}} & D_{\mathrm{two,lno}} & D_{\mathrm{two,lni}} \\ 0 & 0 & I & 0 & D_{\mathrm{twu,lno}} & D_{\mathrm{twu,lni}} \end{bmatrix}; \tag{32}$$

$$B = \begin{bmatrix} B_{\mathrm{lnu,twv}} & B_{\mathrm{lnu,two}} & 0 & I & 0 & 0 \\ B_{\mathrm{lno,twv}} & B_{\mathrm{lno,two}} & B_{\mathrm{lno,twu}} & 0 & I & 0 \\ B_{\mathrm{lni,twv}} & B_{\mathrm{lni,two}} & B_{\mathrm{lni,twu}} & 0 & 0 & I \end{bmatrix}. \tag{33}$$

The zero entries at position $(3,4)$ in D and $(1,3)$ in B are due to the application of the priority rules, e.g. because a fundamental cut-set associated with a current-driven twig can not contain voltage-driven branches because these have a higher priority. The symmetry property of the fundamental cut-set and loop matrices carries over to their subblocks: $B_{a,b} = -D_{b,a}^T$ for any subscripts a and b.

The known voltage drops and known currents of the independent sources are collected in the vectors $\Delta\underline{V}_{\mathrm{twv}}$ and $\underline{I}_{\mathrm{lni}}$ respectively. The voltage-current relations are based on the positive-definite diagonal matrices G_{two}, G_{lnu}, R_{twu}, R_{lno} and the coupling terms $\underline{q}_{\mathrm{two,coup}}$, $\underline{q}_{\mathrm{lnu,coup}}$, $\underline{p}_{\mathrm{twu,coup}}$ and $\underline{p}_{\mathrm{lno,coup}}$. Two sets of unknowns are introduced: the voltage drops $\Delta\underline{V}_{\mathrm{two}}$ along the voltage-driven twigs and the currents $\underline{I}_{\mathrm{lno}}$ through the current-driven links. The currents through the current-driven twigs are

$$\underline{I}_{\mathrm{twu}} = -D_{\mathrm{twu,lno}}\underline{I}_{\mathrm{lno}} - D_{\mathrm{twu,lni}}\underline{I}_{\mathrm{lni}} \tag{34}$$

whereas the voltage drops along the voltage-driven links are

$$\Delta\underline{V}_{\mathrm{lnu}} = -B_{\mathrm{lnu,two}}\Delta\underline{V}_{\mathrm{two}} - B_{\mathrm{lnu,twv}}\Delta\underline{V}_{\mathrm{twv}} \ . \tag{35}$$

The expressions (30), (31), (34) and (35) are substituted into (28) and (29) yielding a mixed formulation for the circuit problem:

$$\begin{bmatrix} G^*_{\mathrm{two}} & D_{\mathrm{two,lno}} \\ -B_{\mathrm{lno,two}} & -R^*_{\mathrm{lno}} \end{bmatrix} \begin{bmatrix} \Delta\underline{V}_{\mathrm{two}} \\ \underline{I}_{\mathrm{lno}} \end{bmatrix} + \begin{bmatrix} \underline{q}^*_{\mathrm{two,coup}} \\ \underline{p}^*_{\mathrm{lno,coup}} \end{bmatrix} = \begin{bmatrix} -\underline{I}_{\mathrm{two,src}} \\ \Delta\underline{V}_{\mathrm{lno,src}} \end{bmatrix} \ , \tag{36}$$

with the positive-definite Schur complements, coupling terms and source terms

$$\begin{aligned}
G^*_{\mathrm{two}} &= G_{\mathrm{two}} - D_{\mathrm{two,lnu}}G_{\mathrm{lnu}}B_{\mathrm{lnu,two}} \ ; && (37)\\
R^*_{\mathrm{lno}} &= R_{\mathrm{lno}} - B_{\mathrm{lno,twu}}R_{\mathrm{twu}}D_{\mathrm{twu,lno}} \ ; && (38)\\
\underline{q}^*_{\mathrm{two,coup}} &= \underline{q}_{\mathrm{two,coup}} - D_{\mathrm{two,lnu}}\underline{q}_{\mathrm{lnu,coup}} \ ; && (39)\\
\underline{p}^*_{\mathrm{lno,coup}} &= \underline{p}_{\mathrm{lno,coup}} - B_{\mathrm{lno,twu}}\underline{p}_{\mathrm{twu,coup}} \ ; && (40)\\
\underline{I}_{\mathrm{two,src}} &= D_{\mathrm{two,lni}}\underline{I}_{\mathrm{lni}} - D_{\mathrm{two,lnu}}G_{\mathrm{lnu}}B_{\mathrm{lnu,twv}}\Delta\underline{V}_{\mathrm{twv}} \ ; && (41)\\
\Delta\underline{V}_{\mathrm{lno,src}} &= B_{\mathrm{lno,twv}}\Delta\underline{V}_{\mathrm{twv}} - B_{\mathrm{lno,twu}}R_{\mathrm{twu}}D_{\mathrm{twu,lni}}\underline{I}_{\mathrm{lni}} \ . && (42)
\end{aligned}$$

The symmetry of the system (36) follows from the property $B_{a,b} = -D_{b,a}^T$. The spectrum of the system contains n_{two} positive eigenvalues and n_{lno} negative eigenvalues with n_{two} the number of voltage-driven twigs and n_{lno} the number of current-driven links.

The magnetic-field, electric circuit coupling is based on this topological circuit description. Solid conductors are catalogued as voltage-driven branches since (9) is of the form (30), whereas stranded conductors, foil windings and multi-conductors have to be treated as current-driven branches due to the expressions (14) and (24) which are similar to (31). The field-circuit coupled system is

$$\begin{bmatrix} K_{\mathrm{fe}} + \jmath\omega L_{\mathrm{fe}} & Z_{\mathrm{fe,mc}} & Q^*_{\mathrm{fe,two}} & P^*_{\mathrm{fe,lno}} \\ Z^T_{\mathrm{fe,mc}} & G_{\mathrm{mc}} & & S^*_{\mathrm{mc,lno}} \\ Q^{*T}_{\mathrm{fe,two}} & 0 & \chi G^*_{\mathrm{two}} & \chi D_{\mathrm{two,lno}} \\ P^{*T}_{\mathrm{fe,lno}} & S^{*T}_{\mathrm{mc,lno}} & -\chi B_{\mathrm{lno,two}} & -\chi R^*_{\mathrm{lno}} \end{bmatrix} \begin{bmatrix} \underline{u} \\ \underline{v} \\ \Delta\underline{V}_{\mathrm{two}} \\ \underline{I}_{\mathrm{lno}} \end{bmatrix} = \begin{bmatrix} \underline{f}_{\mathrm{src}} \\ \underline{g}_{\mathrm{src}} \\ \chi\underline{I}_{\mathrm{two,src}} \\ -\chi\Delta\underline{V}_{\mathrm{lno,src}} \end{bmatrix} \ . \tag{43}$$

The conductances of the solid conductors and the resistances of the stranded conductors, foil windings and general multi-conductors are inserted in G_{two}, R_{lno}, G_{lnu} and R_{twu} depending whether the corresponding circuit branches are twigs or links and eliminated or not. The coupling matrices are denoted similarly as in the previous section but here combine the coupling terms of all conductors present in the FE model. The elimination of solid-conductor links, stranded-conductors twigs, foil-winding twigs and multi-conductor twigs is equivalent to the elimination of the similar non-coupled circuit links and twigs. The corresponding transformed coupling matrices and additional load terms are

$$\begin{aligned}
Q^*_{\mathrm{fe,two}} &= Q_{\mathrm{fe,two}} - Q_{\mathrm{fe,lnu}}B_{\mathrm{lnu,two}} \ ; && (44)\\
P^*_{\mathrm{fe,lno}} &= P_{\mathrm{fe,lno}} - P_{\mathrm{fe,twu}}D_{\mathrm{twu,lno}} \ ; && (45)\\
S^*_{\mathrm{mc,lno}} &= S_{\mathrm{mc,lno}} - S_{\mathrm{fe,twu}}D_{\mathrm{twu,lno}} \ ; && (46)\\
\underline{f}_{\mathrm{src}} &= Q_{\mathrm{fe,lnu}}B_{\mathrm{lnu,twv}}\Delta\underline{V}_{\mathrm{twv}} + P_{\mathrm{fe,twu}}D_{\mathrm{twu,lni}}\underline{I}_{\mathrm{lni}} \ ; && (47)\\
\underline{g}_{\mathrm{src}} &= S_{\mathrm{mc,twu}}D_{\mathrm{twu,lni}}\underline{I}_{\mathrm{lni}} \ . && (48)
\end{aligned}$$

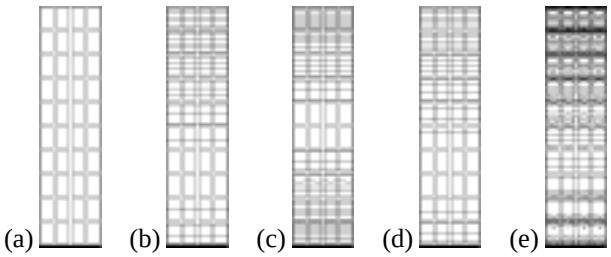

Fig. 8. (a) Geometry, (b) real and (c) imaginary components of the magnetic flux in a single-layer stator slot at 50 Hz and (d) real and (e) imaginary components of the magnetic flux in the multi-conductor model at 500 Hz.

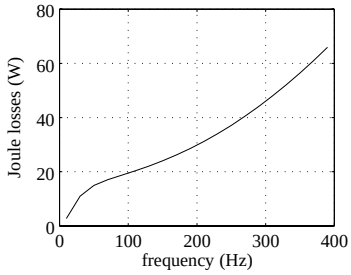

Fig. 9. Harmonic losses in a stator winding of an induction machine.

The field-circuit coupling scheme presented here, is substantially more complicated than more common field-circuit coupling approaches described in literature, such as e.g. modified nodal analysis [12] and loop analysis [6]. The topological approach proposed here, however, allows the treatment of circuit in which voltage-driven coupled branches such as solid conductors and current-driven coupled branches such as stranded conductors, foil windings and multi-conductors may be interconnected in an arbitrary way. Moreover, the approach chosen here, has a rigid mathematical foundation. Writing the KCL only for the fundamental cut-sets and the KVL only for the fundamental loops leads to the system that is proved to be non-singular. The use of both voltage drops and currents as circuit unknowns leads to a circuit system part which is symmetric but indefinite. If a positive definite circuit formulation is favoured, e.g. because the FE formulation itself is also positive definite, the loops equation may be used to eliminate the current unknowns. In that case, however, the positive definite but dense matrices $P^*_{\mathrm{fe,lno}}\frac{1}{\chi}P^{*T}_{\mathrm{fe,lno}}$ and $S^*_{\mathrm{mc,lno}}\frac{1}{\chi}P^{*T}_{\mathrm{mc,lno}}$ have to be added to the FE stiffness matrix $K_{\mathrm{fe}}+\jmath\omega L_{\mathrm{fe}}$ and the foil and multi-conductor conductance matrix G_{mc}. The resulting system of equations can be solved by the Conjugate Gradient method. Due to the loss of the sparsity of these FE system matrices, however, the iterative solver will be considerably more expensive. For symmetric indefinite matrices well-established iterative solution techniques exist as well: as e.g. the symmetric Quasi-Minimal Residual method [5] combined with a block-Jacobi preconditioner [4]. A multi-level solver for field-circuit coupled problems based on this formulation has been developed as well and is described in [8].

Applications

The foil conductor model is applied to simulate the short-circuit operation of a dry-type, three-phase foil-winding distribution transformer (Fig. 4a). The individual foils are not considered by the mesh of the model. The secondary foil windings, each with 50 turns, are connected to additional resistors modelling the contact resistances. The foil and wire windings are embedded in an electrical circuit model (Fig. 1a). The magnetic field is shown in Fig. 1b and Fig. 1c. The current and voltage distributions in one phase of the secondary windings are shown in Fig. 4c and Fig. 4d. A transformer model equipped with the novel treatment for foil windings is compared to a conventional model considering all geometrical details and electric connections of the individual foils by a series connection of solid conductor models. It can be observed in Fig. 7 that the FE discretization error of the foil conductor models with 6, 11 and 21 foil elements, converges significantly faster than the conventional model. By using the novel foil conductor model, the computation time is reduced by a factor of 100 when compared to the conventional model.

The multi-conductor model is also applied to simulate the harmonic losses in induction machine windings [10] (Fig. 8). Since these devices are supplied by variable frequency, the relative importance of the higher harmonic distortion increases and the additional Joule losses are not negligible. These effects are commonly taken into account in analytical models by the frequency dependent eddy current factor which can be provided by a finite element model of a single stator slot [9]. A leakage flux impinging on the conductor is applied to the model by a difference in magnetic vector potential between the top and the bottom of the slot. A conventional model considers the true geometry consisting of the conductors, the insulation and the cooling ducts. It treats the coil as a series connection of a number of solid conductors, each with their own unknown voltage. For many cases, the multi-conductor model offers a sufficient accuracy while avoiding an excessive amount of mesh nodes and voltage unknowns. Adaptive mesh refinement for both the magnetic vector potential and the voltage distribution introduces additional degrees of freedom only at places where they significantly improve the accuracy. The error indicator determines whether the discretization error for the magnetic vector potential and the voltage distribution is sufficiently low. For practical models, this is already attained for an electric mesh which is consid-

erably coarser when compared to the true inner geometry of the multi-conductor system. At 50 Hz, no significant skin effect is observed. At 500 Hz, substantial losses are introduced. The multi-conductor model equipped with independent mesh refinement and external circuit coupling, enables the simulation of the model for all possible frequencies by the same conductor model (Fig. 9).

Conclusions

Discretizing the detailed winding geometry itself and allowing for independent refinement of magnetic and electric meshes results in a considerable saving of degrees of freedom and hence, computation time. As a consequence, foil and multi-conductor models enable a faster, more convenient and more reliable simulation of eddy current effects in windings with complicated shapes compared to common solid and stranded conductor models. The simulation of a foil winding transformer with specialized conductor models requires 10 times less memory and 100 times less computation time.

Acknowledgements

H. De Gersem is working in the cooperation project “DA-WE1 (TEMF/GSI)” with the “Gesellschaft für Schwerionenforschung (GSI)”, Darmstadt. The authors are also grateful to the Belgian "Fonds voor Wetenschappelijk Onderzoek Vlaanderen" (project G.0427), the Belgian Ministry of Scientific Research (IUAP No. P4/20 on Coupled Problems in Electromagnetic Systems) and the Research Council of the Katholieke Univeriteit Leuven for the financial support of a part of this work.

References

[1] L.O. Chua and P.M. Lin, *Computer aided analysis of electronic circuits - algorithms and computational techniques*, Prentice-Hall, New Jersey, 1975.

[2] H. De Gersem and K. Hameyer, *A finite element model for foil winding simulation*, IEEE Transactions on Magnetics **37** (2001), no. 5, 3427–3432.

[3] ———, *A multi-conductor model for finite element eddy current simulation*, IEEE Transactions on Magnetics **38** (2002), no. 2, 533–536.

[4] H. De Gersem, R. Mertens, D. Lahaye, S. Vandewalle, and K. Hameyer, *Solution strategies for transient, field-circuit coupled systems*, IEEE Transactions on Magnetics **36** (2000), no. 4, 1531–1534.

[5] R. Freund and N.M. Nachtigal, *A new Krylov-subspace method for symmetric indefinite linear systems*, Proceedings of the 14th IMACS World Congress on Computational and Applied Mathematics (W.F. Ames, ed.), 1994, pp. 1253–1256.

[6] J. Gyselinck and J. Melkebeek, *Numerical methods for time stepping coupled field-circuit systems*, Proceedings of the International Conference on Modelling and Simulation of Electric Machines, Converters and Systems (ELECTRIMACS 96) (Saint-Nazaire, France), vol. 1, September 1996, pp. 227–234.

[7] A. Kladas and A. Razek, *Numerical calculation of eddy-currents and losses in squirrel cage induction motors due to supply harmonics*, Proceedings of the International Conference on Electrical Machines (ICEM88) (Pisa, Italy), vol. 2, September 1988, pp. 65–69.

[8] D. Lahaye, K. Hameyer, and S. Vandewalle, *An algebraic multilevel preconditioner for field-circuit coupled problems*, Proceedings of the XIIIth Conference on the Computation of Electromagnetic Fields (COMPUMAG2001) (Evian, France), vol. 3, July 2001, pp. 108–109.

[9] R. Richter, *Die Induktionsmaschinen*, 2 ed., Elektrische Maschinen, vol. 4, Birkhauser, Basel, 1963.

[10] S.J. Salon and L. Ovacik ad J.F. Balley, *Finite element calculation of harmonic losses in AC machine windings*, IEEE Transactions on Magnetics **29** (1993), no. 2, 1442–1445.

[11] Á. Szűcs and A. Arkkio, *Consideration of eddy currents in multi-conductor windings using the finite element method and the elimination of inner nodes*, IEEE Transactions on Magnetics **35** (1999), no. 3, 1147–1150.

[12] I.A. Tsukerman, A. Konrad, G. Meunier, and J.C. Sabonnadière, *Coupled field-circuit problems: trends and accomplishments*, IEEE Transactions on Magnetics **29** (1993), no. 2, 1701–1704.

[13] S. Yuferev and N. Ida, *Selection of the surface impedance boundary conditions for a given problem*, IEEE Transactions on Magnetics **35** (1999), no. 3, 1486–1489.